SUPPLEMENTAL INFORMATION

Central π-Conjugated Extension in Quinoxaline-based Small-Molecule Acceptors as Guest Components Enabling High-Performance Ternary Organic Solar Cells

Chung Hang Kwok[#,1,2,3], Ho Ming Ng[#,1,2,3], Chuanlin Gao[4], Huawei Hu[,5], Top Archie Dela Peña[6,7], Joshua Yuk Lin Lai[2,3], Li Chen[2,3], Lan Xie[2,3], Mingjie Li[7], Jiaying Wu[6,8], Guangye Zhang[4], Wai-Yeung Wong*[,1,9], He Yan*[,2,3,10], Han Yu*[,1,2,3]*

[#] *These authors contributed equally.*
** Corresponding authors*

[1] Department of Applied Biology and Chemical Technology, The Hong Kong Polytechnic University, Hung Hom, Hong Kong, PR China
[2] Department of Chemistry, Guangdong-Hong Kong-Macao Joint Laboratory of Optoelectronic and Magnetic Functional Materials, Energy Institute and Hong Kong Branch of Chinese National Engineering Research Center for Tissue Restoration & Reconstruction, Hong Kong University of Science and Technology, Clear Water Bay, Kowloon, Hong Kong, 999077 China
[3] Guangdong-Hong Kong Joint Laboratory for Carbon Neutrality, Jiangmen Laboratory of Carbon Science and Technology, Jiangmen, Guangdong Province, 529199 China
[4] College of New Materials and New Energies, Shenzhen Technology University, Shenzhen, China
[5] State Key Laboratory for Modification of Chemical Fibers and Polymer Materials, College of Materials Science and Engineering, Donghua University, Shanghai 201620, China
[6] Function Hub, Advanced Materials Thrust, The Hong Kong University of Science and Technology, Nansha, 511400 Guangzhou, P. R. China
[7] Department of Applied Physics, The Hong Kong Polytechnic University, Kowloon, Hong Kong, 999077 P. R. China
[8] School of Engineering, Department of Chemical Engineering, The Hong Kong University of Science and Technology, Kowloon, Hong Kong, 999077 P. R. China
[9] Research Institute for Smart Energy, The Hong Kong Polytechnic University, Hung Hom, Hong Kong, PR China
[10] Hong Kong University of Science and Technology-Shenzhen Research Institute, No. 9, Yuexing 1st RD, Hi-tech Park, Nanshan, Shenzhen, 518057 China

CONTENTS

1. Experimental methods

Synthesis and characterization of materials. PM6 was purchased from Solarmer Energy Inc. All other reagents and chemicals were purchased from commercial sources and used without further purification. ^{1}H spectra were obtained with a Bruker AV-400 MHz NMR spectrometer. Chemical shifts were reported in parts per million (ppm, δ), ^{1}H spectra were referenced to tetramethylsilane (0 ppm) in $CDCl_3$. Mass spectra were collected on a MALDI Micro MX mass spectrometer, or an API QSTAR XL System.

Optical and electrochemical characterization. Film UV–Vis absorption spectra were acquired on a Perkin Elmer Lambda 20 UV/VIS Spectrophotometer. All film samples were spin-cast on ITO substrates. Photoluminescence experiment was conducted on a Renishaw MicroRaman/Photoluminescence System. Cyclic voltammetry was carried out on a CHI610E electrochemical workstation with the three electrodes configuration, using Ag/AgCl as the reference electrode, a Pt plate as the counter electrode, and a glassy carbon as the working electrode. 0.1 mol L^{-1} tetrabutylammonium hexafluorophosphate in anhydrous acetonitrile was used as the supporting electrolyte. The polymer and small molecules were drop-cast onto the glassy carbon electrode from chloroform solutions (5 mg mL^{-1}) to form thin films. Potentials were referenced to the ferrocenium/ferrocene couple by using ferrocene as external standards in acetonitrile solutions. The scan rate is 100 mV s^{-1}. The conversion of reduction/oxidation onsets and LUMO/HOMO energy levels can be described as

$$E_{\mathrm{LUMO}} = -\left[e\left(E^{\mathrm{red}} - E^{\mathrm{Fc/Fc+}}\right) + 4.8\right]$$
$$E_{\mathrm{HOMO}} = -\left[e\left(E^{\mathrm{ox}} - E^{\mathrm{Fc/Fc+}}\right) + 4.8\right]$$

Density-functional theory (DFT) calculations. All DFT calculations were performed at the B3LYP/6-311++g(d,p) basis set with the Gaussian 09 package[39].

Device fabrication and testing. OSCs were made with a device structure of glass/ITO (indium tin oxide)/PEDOT:PSS(poly(3,4-ethylenedioxythiophene):poly(styrene sulfonate))/PM6:acceptors/PNDIT-F3N ([(9,9-bis(3'-(N,N-dimethylamino)propyl)-2,7-fluorene)-alt-5,5'-bis(2,2'-thiophene)-2,6-naphthalene-1,4,5,8-tetracaboxylic-N,N'-di(2-ethylhexyl)imide])/Ag. The patterned ITO-coated glass substrates were cleaned in detergent, de-ionized water, acetone, and isopropanol sequentially by ultra-sonic bath for 30 minutes, respectively, and then dried in an oven at 70 ^{o}C overnight. Further UV-ozone treatment for 15 min was applied before use to improve its wettability. Then the PEDOT:PSS (Heraeus Clevios P VP. AI 4083, filtered at 0.45 μm) was spin-coated onto the cleaned ITO-coated glass substrate at 5000 rpm for 30 s followed by annealing at 150 ^{o}C for 15 minutes in the air to obtain ~30 nm thick film. The PEDOT:PSS-coated ITO substrates were then transferred into an N_2-filled glove box for further device fabrication. PM6 was dissolved in chlorobenzene (CB, the concentration of donor was 10 mg mL^{-1}) and stirred at 60 ^oC for 5 hours to form a donor solution. The acceptor materials (BTP-eC9 blends with Qx-B, Qx-Ac and Qx-Pn) were dissolved in chloroform (CF, the concentration of acceptor was 8 mg mL^{-1}) with the solvent additive of 2,5-dibromo-3,4-difluorothiophene (1.5 % of volume) followed by stirring at 50 ^oC for 3 hours to form the acceptor solution. The BTP-eC9:guest ratio was optimized to be 2:1 (and the overall PM6:BTP-eC9:guest ratio to be 1:0.8:0.4) and PM6 solution was spun followed by the solution of the acceptor, and then the active layer was annealed at 100 ^oC for 5 min *via* SD processing. A thin layer of PNDIT-F3N (~10 nm) was spin-coated onto the active layer, and an Ag electrode (~100 nm) was deposited on top of the electron transfer layer in a thermal evaporator under a vacuum of 1×10^{-5} Pa through a shadow mask. The effective device area was 3.4 mm^2 defined by a metal mask with an aperture aligned with the device area. The current-voltage (J-V) characteristics of the photovoltaic devices were measured by a Keithley 2400 Source Meter under RT in the glove box. The photocurrent was measured under AM 1.5G illumination at 100 mW cm^{-2} using a standard Si solar cell (with KG5 filter) and a readout meter to calibrate the light intensity. EQE spectra were measured using an Enlitech QE-S EQE system equipped with a standard Si diode. Monochromatic light was generated from a Newport 300 W lamp source.

Analysis of charge dynamics processes. Exciton dissociation (P_{diss}) and collection (P_{coll}) efficiencies can be calculated from the relationships between photocurrent (J_{ph}) and effective voltage (V_{eff}). J_{ph} is defined as the difference between the dark current density (J_{D}) and the current density under illumination (J_{L}). The definition of V_{eff} is the absolute value of V_0-V_{appl}, where V_0 refers to the voltage value when $J_{\mathrm{L}} = J_{\mathrm{D}}$ and V_{appl} is the applied voltage. At high V_{eff}, almost all excitons are separated and extracted, and J_{ph} reaches saturation (J_{sat}). Accordingly, η_{diss} and η_{coll} can be determined by $J_{\mathrm{SC}}/J_{\mathrm{sat}}$ and $J_{\mathrm{max}}/J_{\mathrm{sat}}$, respectively, in which J_{max} is the current density at the maximal power output point.

Transient photovoltage (TPV) and photocurrent (TPC) characterizations. The device samples were mounted on a conductive clip and under steady-state illumination from a focused Quartz Tungsten-Halogen Lamp light source. The measurements were performed with a background response similar to open-circuit voltage. An optical perturbation was applied to the devices with a 1 kHz femtosecond pulse laser under 600 nm excitation. The TPV signal was acquired by a digital oscilloscope at open-circuit conditions. TPC signal was measured under approximately short-circuit conditions with 50 Ω impedance. The intensity-dependent TPV and TPC measurements were performed by applying various neutral density filters to tune down the background white light and 750 nm pulse excitation. The TPV lifetime τ was fitted with the monoexponential model under a small perturbation approximation. The charges generated ΔQ by the pulse laser were calculated by the integrated TPC peak. The differential capacitance C is then calculated by the equation $C = \Delta Q/\Delta V_0$, where the ΔV_0 is the amplitude of the pulse-generated TPV signal at the corresponding experimental condition. C was fitted with exponential models as a function of V_{OC} and then integrated with respect to voltage to acquire the carrier density. The TPV lifetime τ under different carrier densities n was then fitted to a power law with exponent λ[40,41].

Transient absorption spectroscopy (TAS). A 50% of the output of a 1 kHz, 1W, 100 fs Ti:sapphire laser system with a 827 nm fundamental (Tsunami oscillator/Spitfire amplifier, Spectra-Physics LLC) was used to pump a commercial collinear optical parametric amplifier (TOPAS-Prime, Light-Conversion LLC) tuned to 800. The pump was depolarized to suppress effects due to polarization-dependent dynamics and attenuated to the specific energy density. The pump was focused to a 1 mm diameter spot at the sample position. The probe was generated using 10% of the remaining output to drive continuum generation in a proprietary crystal and detected on a commercial spectrometer (customized Helios, Ultrafast Systems LLC).

Energy loss analysis. Fourier-transform photocurrent spectroscopy external quantum efficiency (FTPS-EQE) spectra were measured by using a Vertex 70 from Bruker optics and a QTH lamp. The electroluminescence signal was collected with a monochromator and detected with a Si-CCD detector.

Morphological characterization. AFM measurements were performed by using a Scanning Probe Microscope Dimension 3100 in ScanAsyst mode. All film samples were spin-cast on ITO substrates.

GIWAXS measurements were performed at beamline BL16B1 at the Shanghai Synchrotron Radiation Facility. Samples were prepared on Si substrates using identical blend solutions as those used in devices. The 10 KeV X-ray beam was incident at a grazing angle of 0.13o , which maximized the scattering intensity from the samples. The scattered X-rays were detected using a Dectris Pilatus 1-M photon counting detector. Samples were prepared on Si substrates. In-plane and out-ofplane sector averages were calculated using the Nika software package. The uncertainty for the peak fitting of the GIWAXS data is 0.3 Å. The coherence length was calculated using the Scherrer equation: $CL=2\pi K/\Delta q$, where Δq is the full-width at half-maximum of the peak and K is a shape factor (0.9 was used here).

Resonant soft X-ray scattering (R-SoXS) transmission measurements were performed at beamline 11.0.1.2 at the ALS. 2 Samples for R-SoXS measurements were prepared on a PSS modified Si substrate under the same conditions as those used for device fabrication, and then transferred by floating in water to a 1.5×1.5 mm, 100 nm thick Si3N4 membrane supported by a 5×5 mm, 200 mm thick Si frame (Norcada Inc.). Two dimensional scattering patterns were collected on an in-vacuum CCD camera (Princeton Instrument PI-MTE). The beam size at the sample is ~100 mm by 200 mm. The composition variation (or relative domain purity) over the length scales probed can be extracted by integrating scattering profiles to yield the total scattering intensity. The purer the average domains are, the higher the total scattering intensity. Owing to a lack of absolute flux normalization, the absolute composition cannot be obtained by only R-SoXS.

2. Synthetic procedures

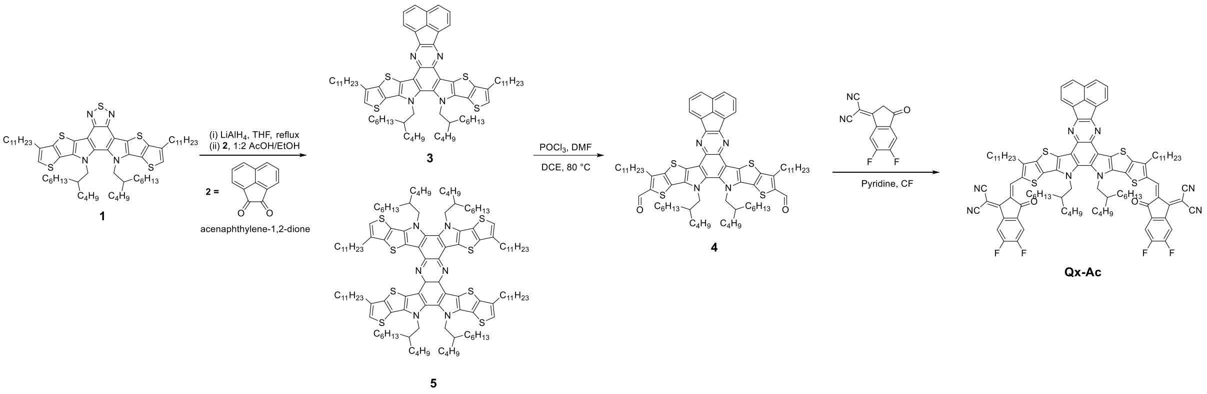

Scheme S1. Synthesis scheme of **Qx-Ac**.

Compound **1** was synthesised according to literature.

Synthesis of compound 3. 220 mg of compound **1** (0.203 mmol) was dissolved in 20 mL of anhydrous tetrahydrofuran. At 0 °C, 154 mg of lithium aluminium hydride (4.1 mmol) was added to the solution. It was allowed to cool to room temperature before heated to reflux overnight. Then, it was quenched by water and filtered through a silica pad. The filtrate was extracted with dichloromethane, dried with Na_2SO_4 and then concentrated under reduced pressure to obtain 100 mg of a crude brownish oil. Without further purification, it was then dissolved in 12 mL of 1:2 acetic acid/ethanol. To the solution was added 18.9 mg of acenaphthylene-1,2-dione (0.104 mmol). The reaction mixture was stirred for 4 hours. After evaporating the solvent, the crude mixture was purified by flash column chromatography (7:1 hexane/dichloromethane) to yield 100 mg of orange-red solid as a mixture of compound **3** and by-product **5**. This mixture is directly used in the next step.

Synthesis of compound 4. The Vilsmeier reagent was prepared by adding 0.4 mL of phosphorus oxychloride to 2 mL of anhydrous *N*,*N*-dimethylformamide at 0 °C. After it was stirred for 30 minutes, it was added to a 10 mL 1,2-dichloroethane solution of the mixture from the previous step at the same temperature. The mixture was then allowed to cool to room temperature before heated at 80 °C. After complete consumption of substrate, the mixture was allowed to return to room temperature before saturated sodium carbonate solution was added and it was stirred for 30 minutes. It was then washed with water, extracted with dichloromethane, dried with anhydrous sodium sulfate and concentrated under reduced pressure. The crude mixture was purified by flash column chromatography (3:1 hexane/dichloromethane) to yield 80 mg of red solid as compound **4** (31% across two steps). **1H NMR** (400 MHz, CDCl3) δ 10.18 (s, 2H), 8.59 (d, J = 6.9 Hz, 2H), 8.11 (d, J = 8.2 Hz, 2H), 7.88 (dd, J = 8.2, 6.9 Hz, 2H), 4.72 (d, J = 7.9 Hz, 4H), 3.28 (t, J = 7.7 Hz, 4H), 2.16 (t, J = 6.3 Hz, 2H), 2.01 (p, J = 7.7 Hz, 4H), 1.54 (p, J = 7.1 Hz, 5H), 1.43 (t, J = 7.1 Hz, 3H), 1.39 – 1.22 (m, 28H), 1.22 – 0.96 (m, 3H), 0.97 – 0.80 (m, 8H), 0.80 – 0.54 (m, 12H), 1.81 (s, 2H). **MS** (ESI) $[M+H]^+$ m/z calcd. for $C_{78}H_{104}N_4O_2S_4$: 1257.7076. Found: 1257.7061.

Synthesis of Qx-Ac. 40 mg of compound **4** (0.0317 mmol) and 29.2 mg of 2-(5,6-difluoro-3-oxo-2,3-dihydro-1*H*-inden-1-ylidene)malononitrile (0.127 mmol) were dissolved in 8 mL of chloroform. After adding 0.8 mL of pyridine, the mixture was heated to 65 °C for 2 hours. The reaction was terminated by evaporating the solvent under reduced pressure. The mixture was purified by flash column chromatography (2:1 dichloromethane/hexane) and then recrystallisation in methanol to yield 45 mg of greenish blue solid as **Qx-Ac** (84%). **^{1}H NMR** (400 MHz, $CDCl_3$) δ 8.93 (s, 2H), 8.38 (d, *J* = 6.8 Hz, 2H), 8.27 (dd, *J* = 9.9, 6.4 Hz, 2H), 8.07 (d, *J* = 8.1 Hz, 2H), 7.80 (t, *J* = 7.5 Hz, 2H), 7.54 (t, *J* = 7.4 Hz, 2H), 4.91 (d, *J* = 8.0 Hz, 4H), 3.10 (t, *J* = 7.6 Hz, 4H), 2.40 (s, 2H), 1.83 (t, *J* = 7.7 Hz, 5H), 1.58 (s, 7H), 1.47 (d, *J* = 14.6 Hz, 1H), 1.45 – 0.92 (m, 67H), 0.92 – 0.56 (m, 18H). **MS** (ESI) $[M+H]^+$ m/z calcd. for $C_{102}H_{108}F_4N_8O_2S_4$: 1681.7448. Found: 1681.7380.

3. Supplementary tables

Table S1. Optical properties of BTP-eC9, Qx-B, Qx-Ac and Qx-Pn.

	$\lambda_{max,sol}$ (nm)	**$\lambda_{max,film}$ (nm)**	**$\Delta\lambda_{sol,\ film}$ (nm)**	**ε (10^5 M^{-1} cm^{-1})**	**Stokes shift (nm)**	**$\lambda_{onset,film}$ (nm)**	**E_g (eV)**
BTP-eC9	746	837	91	2.37	39	928	1.34
Qx-B	752	818	66	2.03	71	924	1.34
Qx-Ac	749	803	54	2.05	61	888	1.40
Qx-Pn	749	800	51	1.60	60	893	1.39

Table S2. Optimization data of PM6:BTP-eC9:Qx-Ac devices.

PM6:BTP-eC9:Qx-Ac ratio	V_{OC} (V)	**J_{SC} (mA cm^{-2})**	**FF (%)**	**PCE (%)**
1: 1.2: 0	0.843	26.78	77.74	17.55
1: 1: 0.1	0.849	26.74	77.88	17.70
1: 1: 0.2	0.855	26.72	78.11	17.84
1: 0.8: 0.4	0.874	26.69	79.35	18.51
1: 0.6: 0.6	0.887	26.22	75.36	17.53
1: 0: 1.2	0.924	24.71	72.01	16.44

Table S3. Device performances of binary PM6:Qx systems.

	V_{OC} (V)	J_{SC} (mA cm^{-2})	FF (%)	PCE (%)
PM6:Qx-B	0.840	26.17	71.64	15.74
PM6:Qx-Ac	0.924	24.71	72.01	16.44
PM6:Qx-Pn	0.934	23.44	72.47	15.87

Table S4. Morphology parameters extracted from GIWAXS scattering patterns of the blend films.

		Binary and ternary blends			
		PM6:BTP-eC9	**PM6:BTP-eC9:Qx-B**	**PM6:BTP-eC9:Qx-Ac**	**PM6:BTP-eC9:Qx-Pn**
In-plane (100)	q_{xy} **(Å^{-1})**	0.31	0.31	0.31	0.31
	d **(Å)**	20.26	20.26	20.26	20.26
	CCL (nm)	51.4	49.1	55.4	53.3
π-π **stacking (010)**	q_z **(Å^{-1})**	1.75	1.76	1.76	1.76
	d **(Å)**	3.58	3.57	3.58	3.57
	CCL (nm)	34.5	32.3	37.7	36.3

Table S5. Energy loss characteristics of the fabricated devices.

Active layer	**E_g (eV)**	**$qV_{oc}^{meas.}$ (eV)**	**E_{loss} (eV)**	**ΔE_1 (eV) [a]**	**E_{CT}**	**ΔE_2 (eV) [a]**	**ΔE_3 (eV) [a]**
PM6:BTP-eC9	1.409	0.845	0.564	0.261	1.337	0.072	0.231
PM6:BTP-eC9:Qx-B	1.407	0.849	0.558	0.262	1.337	0.070	0.226
PM6:BTP-eC9:Qx-Ac	1.410	0.877	0.533	0.262	1.345	0.065	0.206
PM6:BTP-eC9:Qx-Pn	1.420	0.876	0.544	0.262	1.358	0.062	0.220

[a] **ΔE_1** is the radiative recombination loss; **ΔE_2** is the loss due to charge generation; **ΔE_3** is the non-radiative recombination loss.

4. Supplementary figures

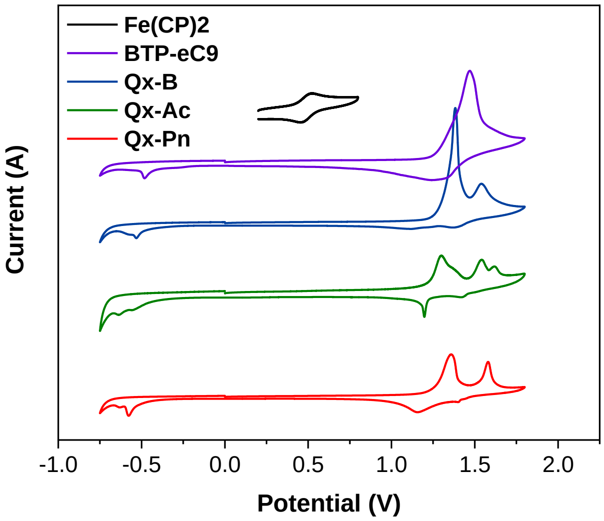

Figure S1. Cyclic voltammogram of the acceptors and Fe(CP)$_2$ as reference.

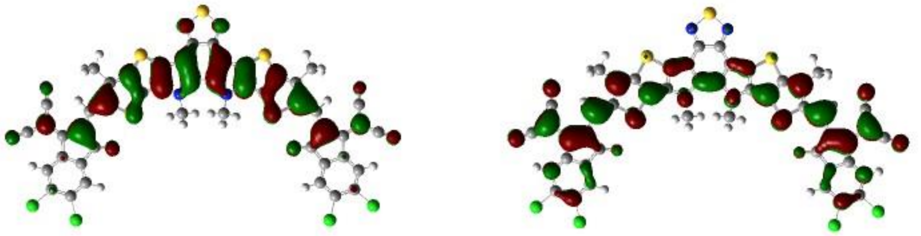

HOMO = -5.96 eV LUMO = -3.95 eV

BTP-eC9

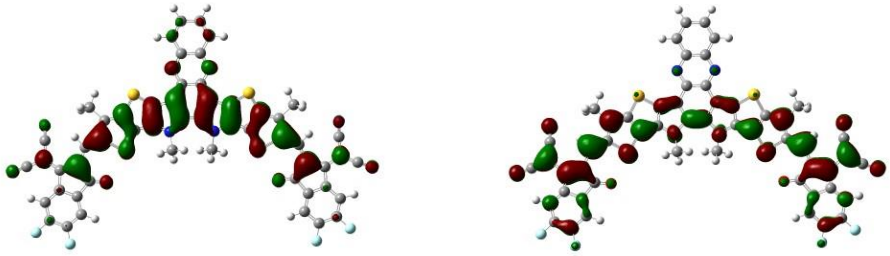

HOMO = -5.87 eV LUMO = -3.88 eV

Qx-B

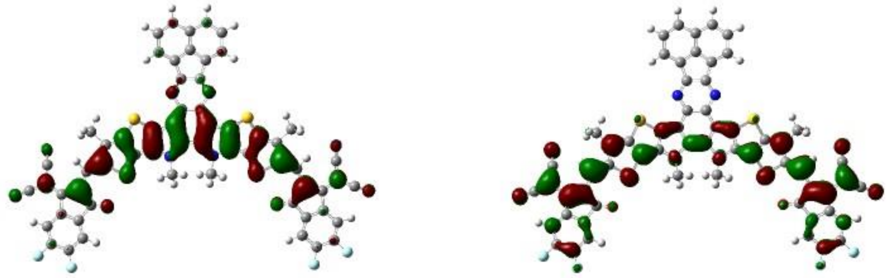

HOMO = -5.83 eV LUMO = -3.83 eV

Qx-Ac

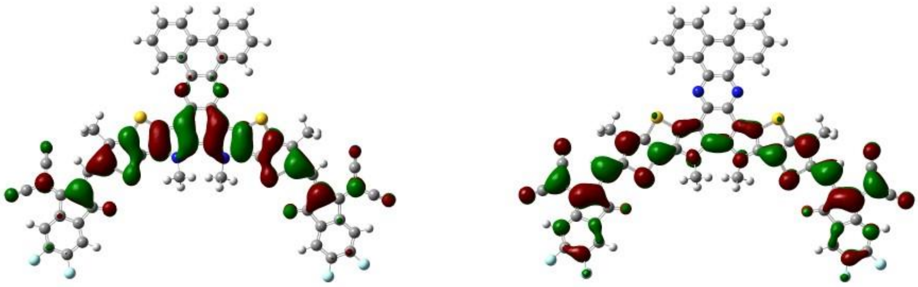

HOMO = -5.84 eV LUMO = -3.83 eV

Qx-Pn

Figure S2. Frontier orbitals of the acceptors, calculated through density-functional theory (DFT) methods.

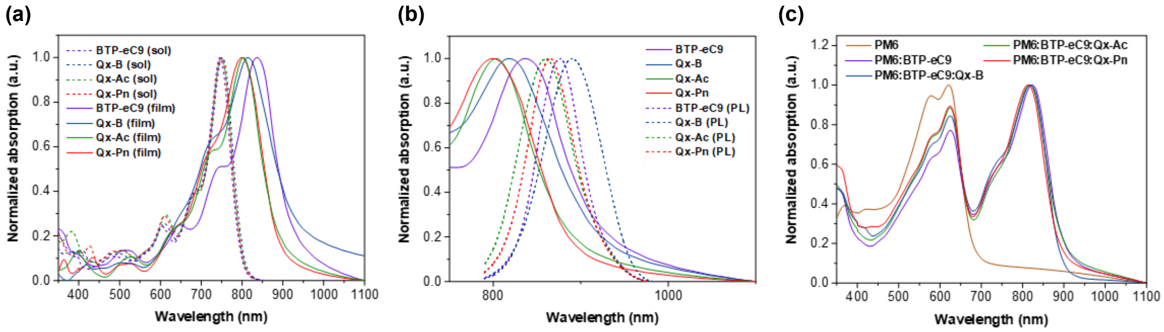

Figure S3. (a) The solution-film absorption shifts of the acceptors. (b) Film absorption spectra of the acceptors with photoluminescence spectra overlaid, showing their Stokes shifts. (c) Absorption spectra of the PM6, the BTP-eC9 binary blend and the ternary blends with Qx-B, Qx-Ac and Qx-Pn as thin films.

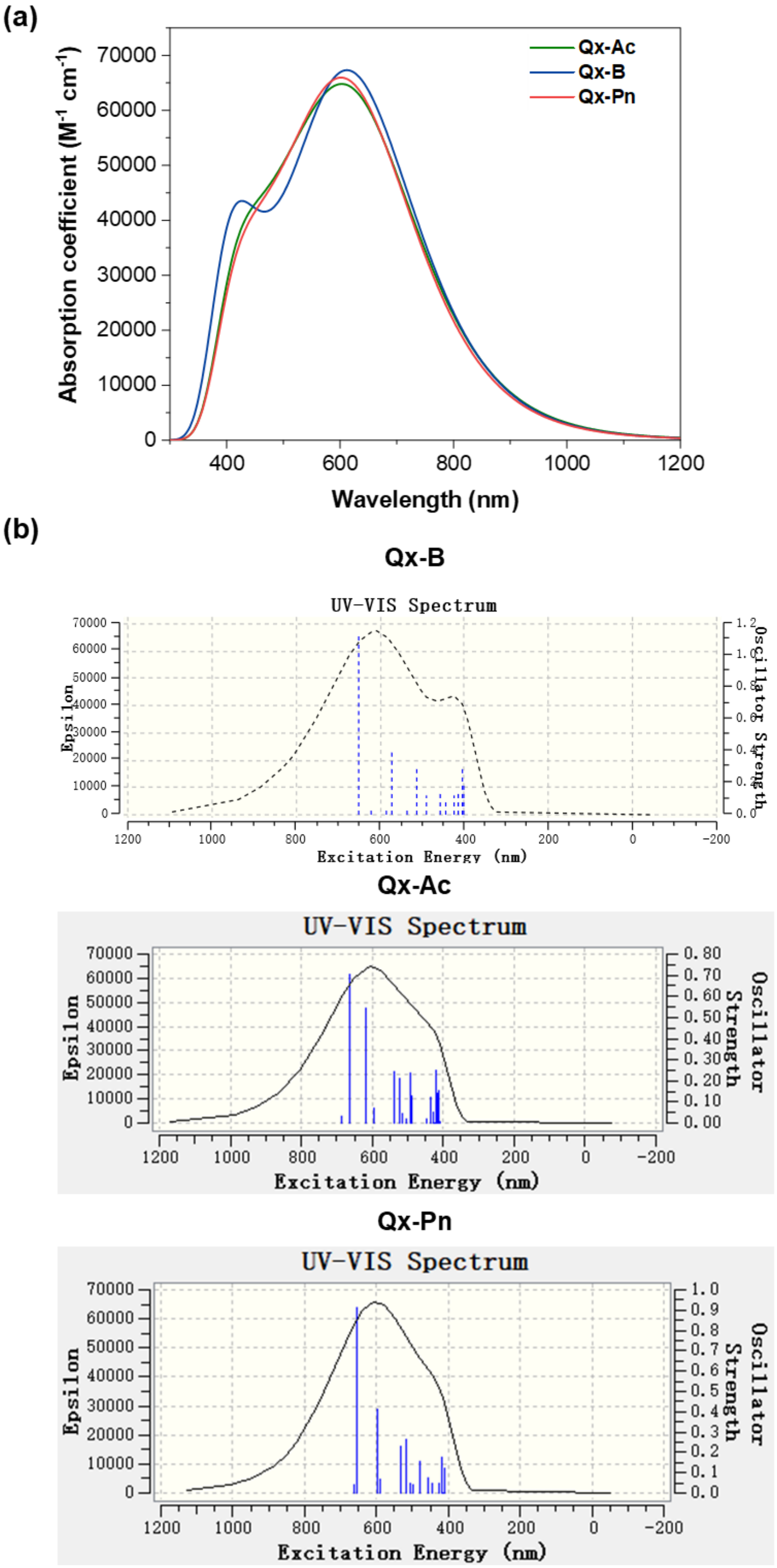

Figure S4. (a) Calculated absorption coefficients and (b) oscillator strengths of the Qx-based acceptors through time-dependent DFT.

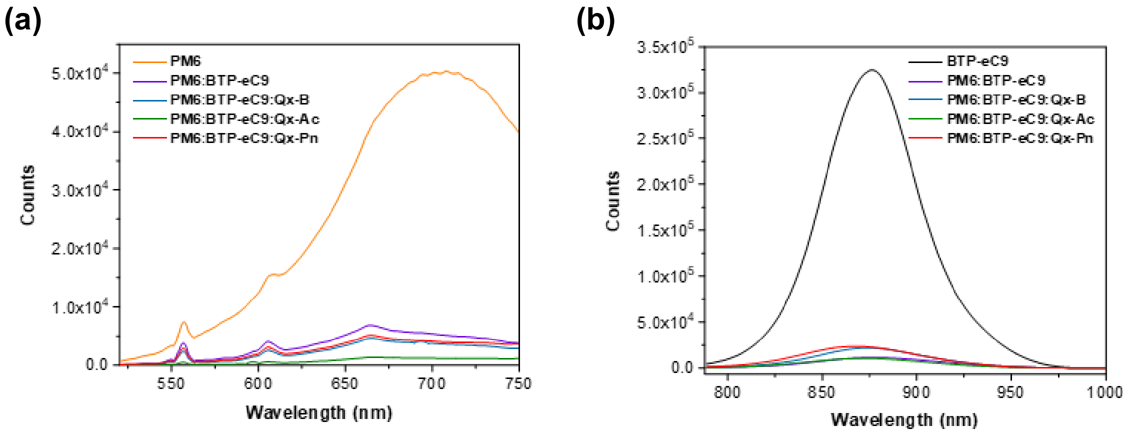

Figure S5. Photoluminescence spectra of the donor and acceptor thin films under (a) 514 nm and (b) 785 nm excitation.

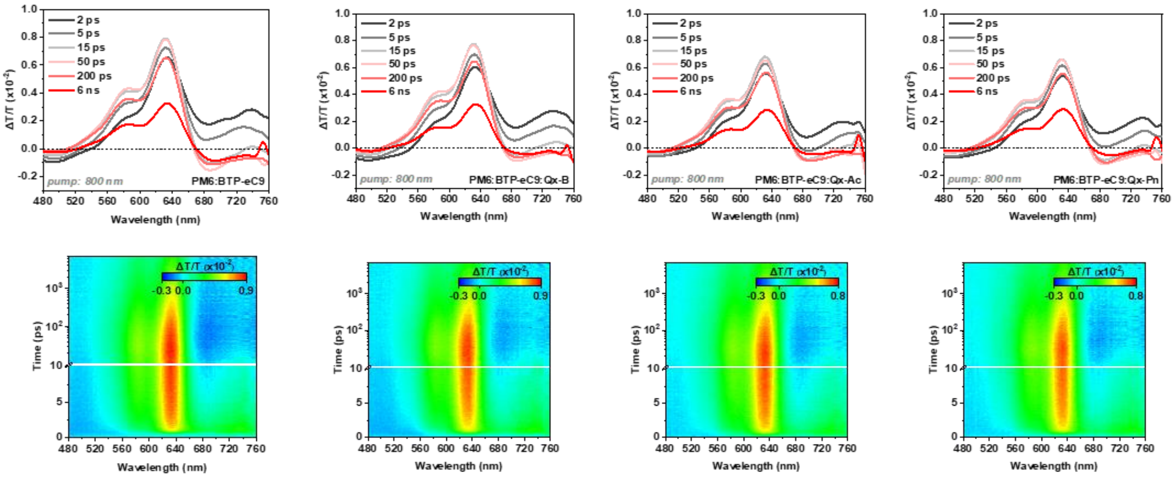

Figure S6. Transient absorption spectra of the BTP-eC9 binary and ternary blends and their 2D contour plot with 800 nm pump wavelength at 2 uJ/cm^2 fluence.

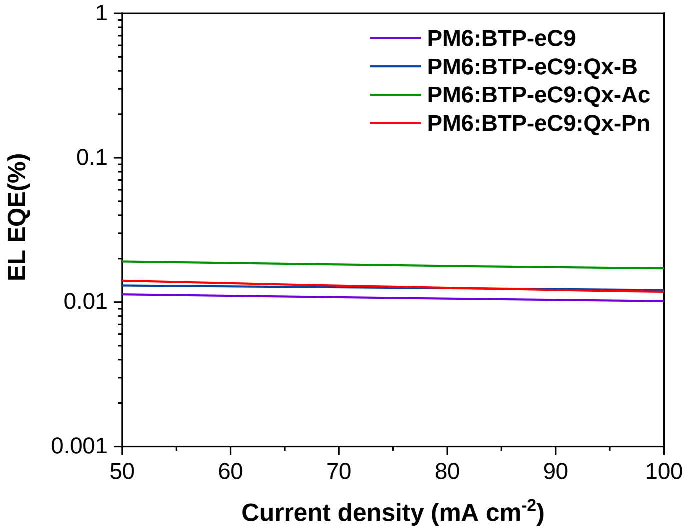

Figure S7. Electroluminescence quantum efficiency (EQE_{EL}) as dependence on current density as a function of energy for devices based on PM6:BTP-eC9, PM6:BTP-eC9:Qx-B, PM6:BTP-eC9:Qx-Ac and PM6:BTP-eC9:Qx-Pn.

5. ^{1}H NMR and mass spectra of compounds

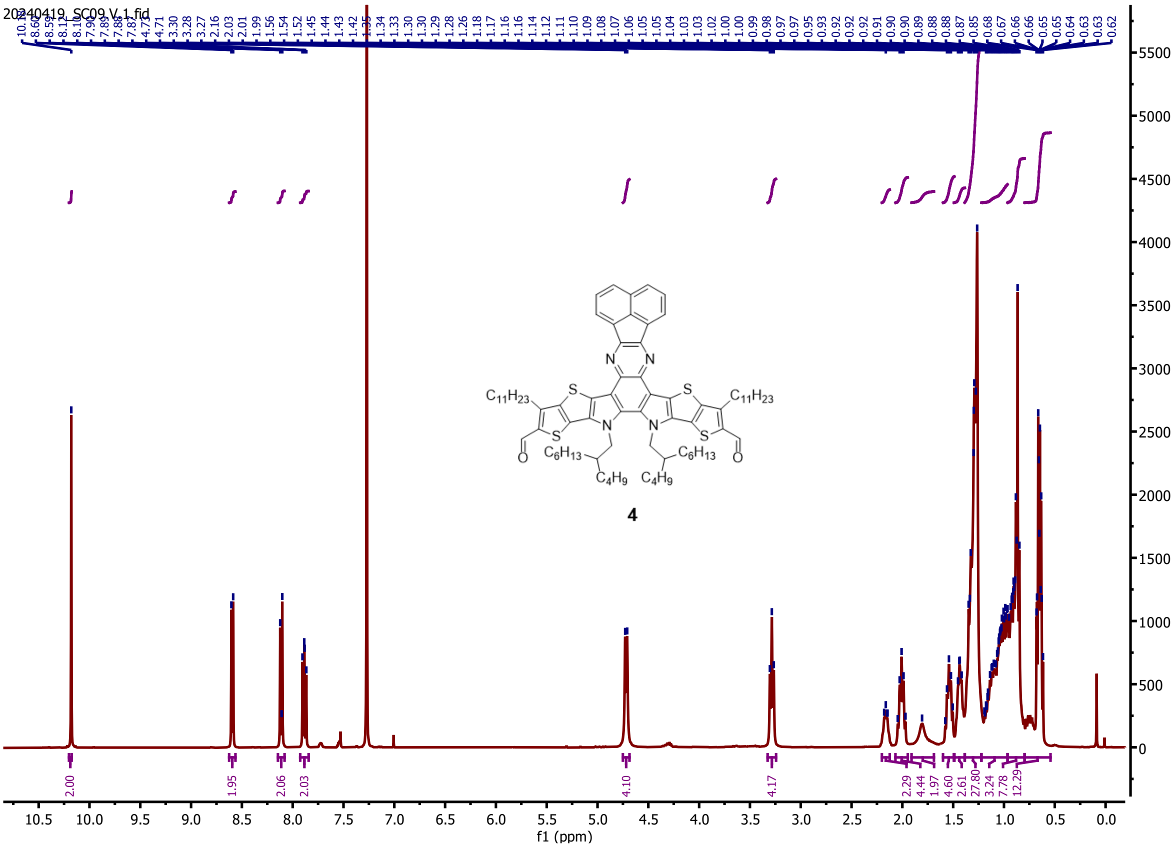

Figure S8. ^{1}H NMR spectrum of compound **4** (400 MHz, $CDCl_3$).

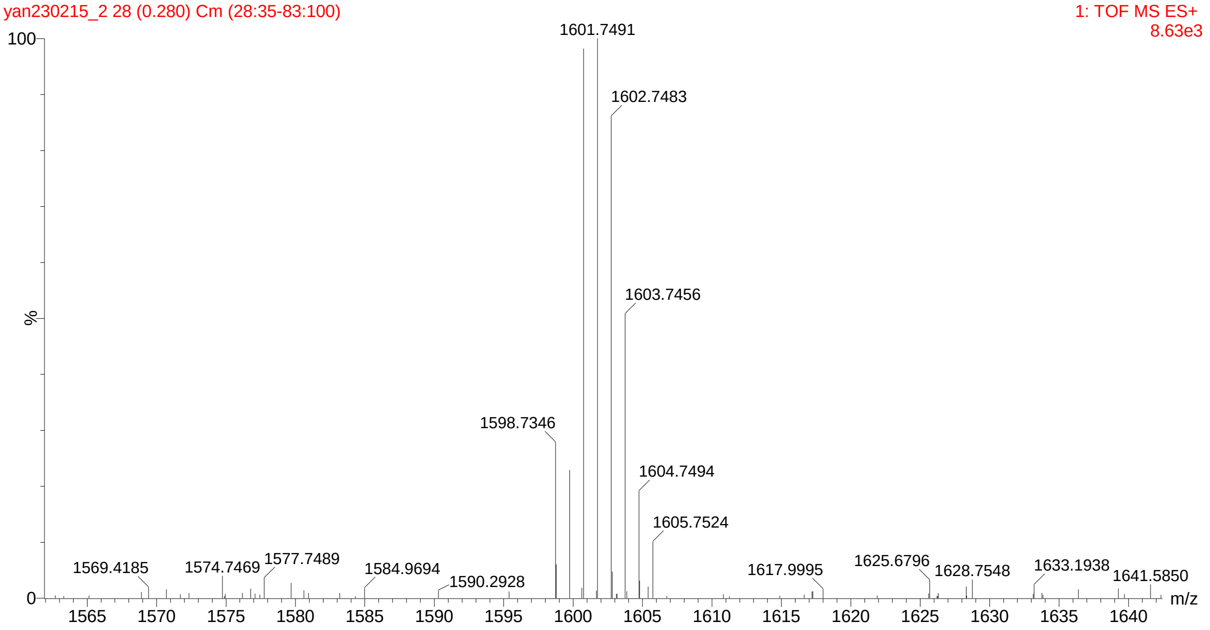

Figure S9. ESI+ MS spectrum of compound **4**.

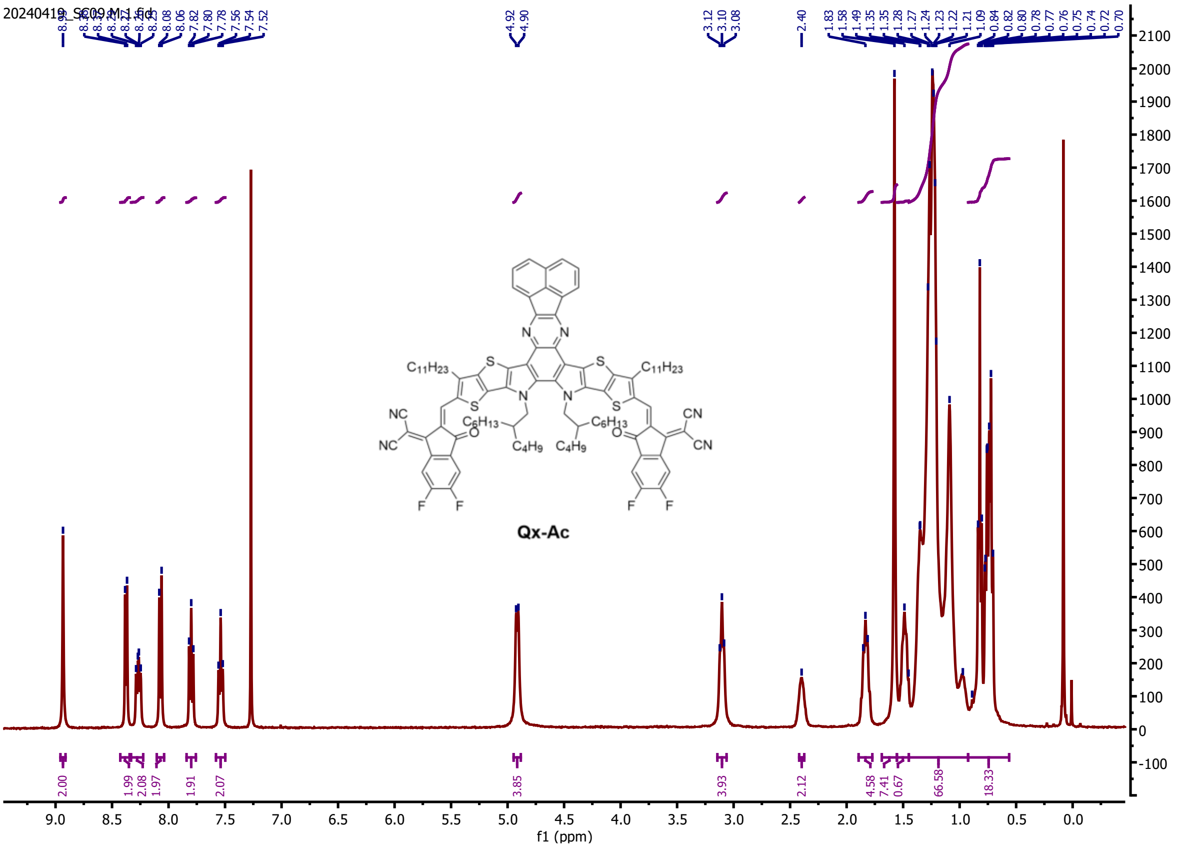

Figure S10. ^{1}H NMR spectrum of **Qx-Ac** (400 MHz, CDCl$_3$).

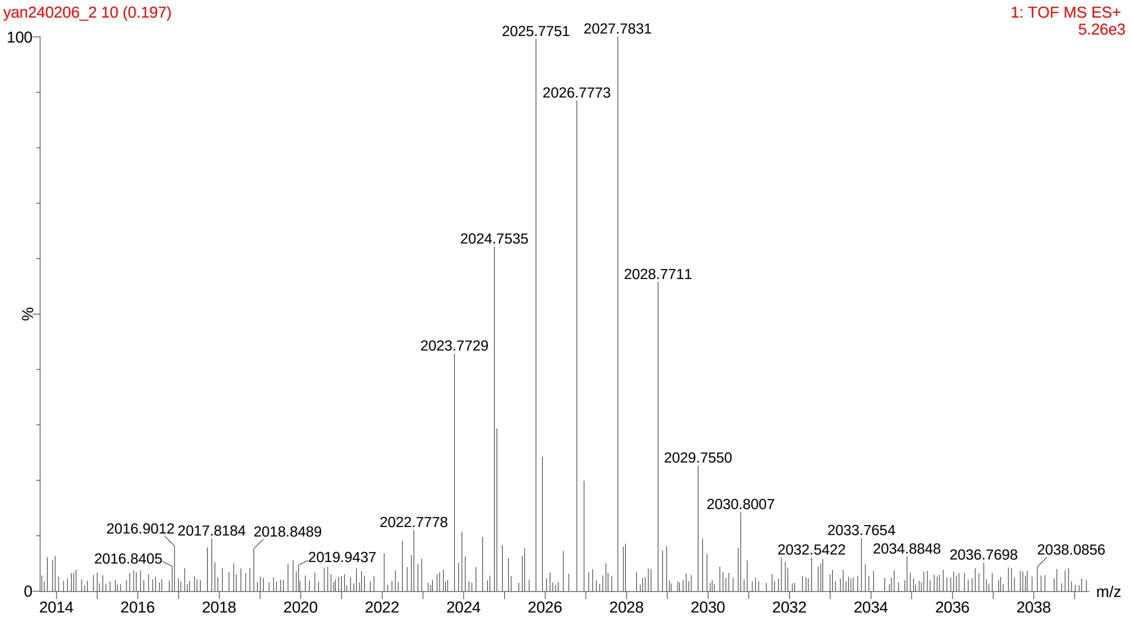

Figure S11. ESI- MS spectrum of **Qx-Ac**.